AD NUMBER

ADB021861

LIMITATION CHANGES

TO:

Approved for public release; distribution is unlimited.

FROM:

Distribution authorized to U.S. Gov't. agencies only; Test and Evaluation; SEP 1977. Other requests shall be referred to Air Force Flight Dyamics Laboratory, FX, Wright-Patterson AFB, OH 45433.

AUTHORITY

AFWAL ltr, 9 Mar 1984

AEDC-TR-77-86

(3)

TRANSITION MEASUREMENTS VIA HEAT-TRANSFER INSTRUMENTATION ON A 0.5 BLUNTNESS 9.75-DEG CONE AT MACH 7 WITH AND WITHOUT MASS ADDITION

VON KÁRMÁN GAS DYNAMICS FACILITY
ARNOLD ENGINEERING DEVELOPMENT CENTER
AIR FORCE SYSTEMS COMMAND
ARNOLD AIR FORCE STATION, TENNESSEE 37389

September 1977

Final Report for Period May 19 – June 8, 1977

Prepared for

AIR FORCE FLIGHT DYNAMICS LABORATORY (FX)
WRIGHT-PATTERSON AFB, OHIO 45433

NOTICES

When U. S. Government drawings specifications, or other data are used for any purpose other than a definitely related Government procurement operation, the Government thereby incurs no responsibility nor any obligation whatsoever, and the fact that the Government may have formulated, furnished, or in any way supplied the said drawings, specifications, or other data, is not to be regarded by implication or otherwise, or in any manner licensing the holder or any other person or corporation, or conveying any rights or permission to manufacture, use, or sell any patented invention that may in any way be related thereto.

Qualified users may obtain copies of this report from the Defense Documentation Center.

References to named commercial products in this report are not to be considered in any sense as an endorsement of the product by the United States Air Force or the Government.

APPROVAL STATEMENT

This technical report has been reviewed and is approved for publication.

FOR THE COMMANDER

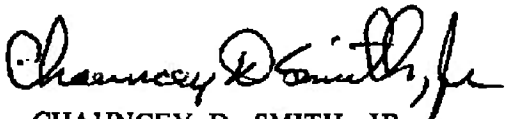

CHAUNCEY D. SMITH, JR.
Lt Colonel, USAF
Director of Test Operations
Deputy for Operations

ALAN L. DEVEREAUX
Colonel, USAF
Deputy for Operations

REPORT DOCUMENTATION PAGE

READ INSTRUCTIONS BEFORE COMPLETING FORM

1 REPORT NUMBER: AEDC-TR-77-86	2 GOVT ACCESSION NO:
3 RECIPIENT'S CATALOG NUMBER:	
4 TITLE (and Subtitle): TRANSITION MEASUREMENTS VIA HEAT-TRANSFER INSTRUMENTATION ON A 0.5 BLUNTNESS 9.75-DEG CONE AT MACH 7 WITH AND WITHOUT MASS ADDITION	5 TYPE OF REPORT & PERIOD COVERED: Final Report - May 19 - June 8, 1977
	6 PERFORMING ORG. REPORT NUMBER:
7 AUTHOR(s): A. H. Boudreau, ARO, Inc.	8 CONTRACT OR GRANT NUMBER(s):
9 PERFORMING ORGANIZATION NAME AND ADDRESS: Arnold Engineering Development Center Air Force Systems Command Arnold Air Force Station, Tennessee 37389	10 PROGRAM ELEMENT, PROJECT, TASK AREA & WORK UNIT NUMBERS: Program Element 62201F Project 1366
11 CONTROLLING OFFICE NAME AND ADDRESS: Air Force Flight Dynamics Laboratory (FX) Wright-Patterson AFB, Ohio 45433	12 REPORT DATE: September 1977 13 NUMBER OF PAGES: 29
14 MONITORING AGENCY NAME & ADDRESS (if different from Controlling Office):	15 SECURITY CLASS. (of this report): UNCLASSIFIED 15a DECLASSIFICATION/DOWNGRADING SCHEDULE: N/A

16 DISTRIBUTION STATEMENT (of this Report)

Distribution limited to U.S. Government agencies only; this report contains information on test and evaluation of military hardware; September 1977; other requests for this document must be referred to Air Force Flight Dynamics Laboratory (FX), Wright-Patterson AFB, Ohio 45433.

17 DISTRIBUTION STATEMENT (of the abstract entered in Block 20, if different from Report)

18 SUPPLEMENTARY NOTES

Available in DDC

19 KEY WORDS (Continue on reverse side if necessary and identify by block number)

transitions	blunt bodies	boundary layer
measurements	conical bodies	Reynolds number
heat transfer	Mach numbers	
instrumentation	mass	

20 ABSTRACT (Continue on reverse side if necessary and identify by block number)

A test was conducted at Mach number 7.2 on a blunt cone featuring porous skins for mass addition to the boundary layer. Transition location was determined in relation to variations of Reynolds number, mass flow, and angle of attack. As expected, transition locations were dependent upon angle of attack for the range of angles tested (0 to 5 deg). However, only the highest mass flow rate of 0.042 lbm/sec injected through the nose

DD FORM 1 JAN 73 1473 EDITION OF 1 NOV 65 IS OBSOLETE

20. ABSTRACT (Continued)

section produced significant effects on the location of transition.

PREFACE

The work reported herein was conducted by the Arnold Engineering Development Center (AEDC), Air Force System Command (AFSC), at the request of the Air Force Flight Dynamics Laboratory (AFFDL), for the General Electric Co., Re-entry and Environmental Systems Division, under Program Element 62201F, Project 1366. The results of the test were obtained by ARO, Inc., AEDC Division (a Sverdrup Corporation Company), operating contractor for the AEDC, AFSC, Arnold Air Force Station, Tennessee, under ARO Project No. V41F-J4A. The author of this report is A. H. Boudreau, ARO, Inc. Clark M. Walker, Lt Colonel, USAF, is Chief of the von Kármán Gas Dynamics Facility Division. Data analysis was completed on July 8, 1977, and the manuscript (ARO Control No. ARO-VKF-TR-77-53) was submitted for publication on August 12, 1977.

CONTENTS

ILLUSTRATIONS

TABLE

1.0 INTRODUCTION

This test was conducted in the Arnold Engineering Development Center (AEDC) Hypervelocity Wind Tunnel (F) (Tunnel F) of the von Kármán Gas Dynamics Facility (VKF). The test objectives were to determine movement of boundary-layer transition as a function of Reynolds number, mass flow, and angle of attack. The test was conducted at a nominal free-stream Mach number of 7.2 and over a free-stream Reynolds number range from 2.8 x 10^6/ft to 40 x 10^6/ft. Angle of attack ranged from 0 to 5 deg, and mass flow ranged from 0.0024 to 0.042 lbm/sec.

2.0 APPARATUS

2.1 WIND TUNNEL

Tunnel F (Fig. 1) is an arc-driven wind tunnel of the hotshot type (Refs. 1 and 2) and capable of providing Mach numbers from about 7 to 20 over a Reynolds number per ft range from 0.05 x 10^6 to 50 x 10^6. Tests can be conducted in a 108-in.-diam conical nozzle or in a family of contoured nozzles. Mach numbers from 18 to 20 can be obtained in the 108-in.-diam test section using the 4-deg half-angle conical nozzle. The range of Mach numbers is obtained by using various throat diameters. Tests utilizing contoured nozzles are conducted at the 54-in.-diam test section over the Mach number range from 7 to 13. The three axisymmetric, contoured nozzles have 25-, 40-, and 48-in. exit diameters which connect to the 54-in.-diam test station and provide a free-jet exhaust (Fig. 2). Nitrogen gas is used for aerodynamic and aerothermodynamic testing; air is used for combustion testing. The test gas is confined in either a 1.0-, 2.5-, or a 4.0-cu-ft arc chamber where it is heated and compressed by an electric arc discharge. The increase in pressure results in a diaphragm rupture with the subsequent flow expansion through the nozzle. Test times are typically from 50 to 200 msec. Shadowgraph and schlieren coverage is available at both test sections.

This test was conducted using the 25-in.-exit-diam contoured nozzle in the 54-in.-diam test section to obtain a nominal free-stream Mach number of 7.2. A tunnel installation sketch is presented in Fig. 3. Nitrogen gas was used for the test. The 4-cu-ft arc chamber was used, and useful test times up to approximately 100 msec were obtained. Because of the relatively short test times, the model wall temperature remained essentially invariant from the initial value of approximately 540°R, thus $T_w/T_o \simeq 0.38$ to 0.54 which approximates the condition of practical interest for reentry vehicles.

2.2 MODEL

The test article (designed and fabricated by the General Electric Co.) is illustrated in Fig. 4 and consists of an $r_n/r_b = 0.5$ bluntness, 9.75-deg half-angle sphere cone. The surface of the model was constructed of porous steel to provide for mass addition to the boundary layer. Two model mass addition chambers with different metal porosities provided a capability of varying the mass addition on the nose and conical sections. In addition, the nose section skin surface featured a varying wall thickness to simulate the variable mass addition per unit area encountered in actual ablation. Independent mass supply lines provided room temperature nitrogen to the two chambers. Instrumentation lead wires were sealed as they entered the hollow support sting in order to prevent leaks. Pressure and temperature were monitored in the mass addition chambers via internally mounted transducers.

Slight leaks, resulting in weak jetting, were present (before testing) around gages and plugs installed in the porus skin. These leaks were sealed by applying Eastman® 910 cement to the outside surface of the model at the leak locations. The sealing process left glue residues around a number of gages.

Although most leaks were successfully sealed, some weak jets were present on all mass flow runs. Strong jets are known to be effective in tripping laminar boundary layers. These jets were, however, relatively weak and thought to have insignificant effects on the location of transition. Observable residues existed around gages 2, 3, 4, 17, 19, 20, 21, 31, 32, 33, 34, 40, and 44 throughout the test. A posttest inspection showed moderate jets around gages 11, 15, 25, 39, 47, 54, 55, and P5 and slight jetting around gages 5, 7, 12, 13, 17, 33, 36, and 57 at a mass flow rate of 0.02 lbm/sec.

2.3 INSTRUMENTATION

Coaxial surface thermocouple gages (see Ref. 2) were used to measure the surface heating rate distributions. The coaxial gage consists of an electrically insulated Chromel® center conductor enclosed in a cylindrical constantan jacket. Thermal and electrical contact between the two materials is established in a thin layer at the surface of the gage, i.e., a surface thermocouple.

In practical measurement applications, the surface thermocouple behaves as a homogeneous, one-dimensional, semi-infinite solid. The instrument provides an electromotive force (EMF) directly proportional to surface temperature which may be related by theory to the incident heat flux. All heat-transfer gages were bench calibrated before installation in the model. The precision of these calibrations is estimated to be ±3 percent. The gages were supplied and installed by the AEDC-VKF.

Model pressures were measured with internally mounted pressure transducers built by VKF. For pressures greater than 1 psid, a wafer-style semiconductor strain-gage transducer with a sealed reference port was used. For pressures less than 1 psid, a similar wafer transducer was used with the reference port at near vacuum pressure. The wafer

transducer is nominally 0.56 in. in diameter by 0.25 in. thick. Application of a differential pressure produces a force on the metal diaphragm. The diaphragm is instrumented with two semiconductor strain gages which sense the deflection.

The test section was instrumented with various probes to monitor the tunnel conditions. The probe systems consisted of two hemisphere cylinders instrumented with coaxial heat-transfer gages and two pitot pressures. The diameter of the test section flow-field hemisphere cylinder heat monitor probes was selected as the maximum size that would still have a laminar boundary layer at the shoulder gage locations. This criterion dictated 3/8-in.-diam probes at $M_\infty = 7.2$. The hemisphere cylinders were instrumented with coaxial surface thermocouples to measure the heat-transfer rate at the stagnation and shoulder location. The pressures measured on the various probes were obtained using standard strain-gage transducers developed at AEDC-VKF. The heat probes and pitot pressure probes were mounted at an appropriate distance from the model to eliminate shock interference. In addition, four static pressure transducers were installed on the wall of the 25-in.-diam nozzle at station 365.

All instrumentation discussed was developed at AEDC specifically for Tunnel F applications. Further description and discussion can be found in Refs. 2, 3, and 4.

3.0 PROCEDURES

3.1 TEST CONDITIONS

The method of determining the tunnel flow conditions is briefly summarized as follows: instantaneous values of nozzle static pressure and pitot pressure (p_o') are measured, and an instantaneous value of the stagnation heat-transfer rate ($\dot{q}_o$) is inferred from a direct measurement

of shoulder heat rates on the hemisphere cylinder heat probes. Total enthalpy (h_o) is calculated from p_o' and $\dot{q}_o$ and the heat probe radius, using the Fay-Riddell theory (Ref. 5). The free-stream static pressure is obtained from the nozzle static pressures in a correlation determined from previous detailed tunnel calibrations. The Mach number is calculated from the isentropic relationship using the test section pitot pressure and static pressure.

The centerline pitot pressure on the test model, the Mach number, and h_o are then used to calculate the free-stream conditions from isentropic flow equations and the normal shock relationships. The isentropic reservoir conditions are read from tabulated thermodynamic data for nitrogen (Ref. 6) using h_o and s_∞/R. The equations for this procedure are contained in Refs. 7 and 8.

Test conditions for this test were:

Condition	~M_∞	~T_o, °R	~$(Re_\infty/ft \times 10^{-6})_{max}$
1	7.2	1,400	10
2	7.0	1,100	20
3	6.9	1,000	40

3.2 TEST PROCEDURES

The primary test variables were angle of attack, mass flow rates, and free-stream Reynolds number. These variables are listed in Table 1. Eleven of the 22 runs featured mass addition.

The mass flow system was automatically triggered 3 sec before the run to allow sufficient time for chamber filling. The mass flow rate remained essentially constant throughout a given run, whereas free-stream conditions varied as described in Section 3.3. The preselected mass flow rates were controlled by setting an initial reservoir pressure

upstream of a calibrated venturi. The mass flow system provided two independently adjustable mass flow lines to the model, with the No. 1 System supplying the nose chamber and the No. 2 System supplying the conical section chamber. The system provided the model with sufficient flow rates of filtered (10 μ), dried (silica gel) nitrogen. Dew point is typically -90°F at atmospheric pressure.

3.3 DATA ACQUISITION AND REDUCTION

The model data (pressure and heat-transfer rate) and the tunnel monitor probe data were recorded on the Tunnel F Transient Data System (TDS). The TDS is capable of scanning the 100 available data channels at preselected rates (normally 100,000 samples/sec). Data for an entire run were stored on the disk unit of a PDP 11/40 Computer which is an integral part of the TDS. The run data plus calibration results and model constants are transmitted to an offline digital computer for final data reduction.

Since Tunnel F operates with a constant volume reservoir with an initial charge density, the reservoir conditions decay with time. As a result, all tunnel conditions and model data results vary with time during the useful data range. Nondimensional values such as M_∞ and model pressure/p_o' are relatively constant with time. Timewise variations in Reynolds number permit acquisition of data at different Reynolds numbers for the same run. Figure 5 indicates the typical timewise variations of test conditions in Tunnel F.

4.0 DATA PRECISION

4.1 TEST CONDITIONS

Laboratory calibration using static loads indicates that the pressure transducers are accurate to ±1 percent. Similarly, the uncertainties in the heat-transfer-rate gages are ±5 percent. The uncertainties in measured data, however, are higher because of the dynamics of the measurements and system errors. The uncertainties in the monitor probe measurements (p_o' and $\dot{q}_o$) were estimated considering both the static load calibrations and the repeatability of the test section pitot profiles. The uncertainty in the pressure data (p_o') is estimated to be ±3 percent, based on an average of two measurements. The heat-transfer-rate ($\dot{q}_o$) uncertainty is ±5 percent based on an average of four measurements. The uncertainty in the Mach number, determined from monitor measurements during each run, is ±3 percent. These values, along with the results from the tunnel calibration, were used to estimate uncertainties in the tunnel flow parameters by the Taylor series method of error propagation. Representative parameters are given below.

Uncertainty (±), percent		
P_∞	T_∞	Re_∞/ft
7	8	11

4.2 MODEL DATA

The uncertainty estimates for the model heat-transfer rate and pressure data are given below in terms of the absolute level measured. The reference heat-transfer rate ($\dot{q}_o$) uncertainty is ±5 percent, and p_o' is ±3 percent. Therefore, the uncertainty of the nondimensional ratio $\dot{q}/\dot{q}_o$ and p/p_o' by the Taylor series method of error propagation yields the following:

$\dot{q}$ Range, Btu/ft^2-sec	Uncertainty (±), percent $\dot{q}$	$\dot{q}/\dot{q}_o$
>1	9	10
0.2 to 1.0	14	15

p Range, psia	p	p/p_o
>0.5	4	5
<0.5	9	10

Model attitude in pitch, yaw, and roll is estimated to be within ±0.10 deg. The mass flow rate ($\dot{m}$) uncertainty is ±5 percent.

5.0 RESULTS AND DISCUSSION

The timewise variation of Reynolds number during a typical Tunnel F run makes it particularly attractive for boundary-layer transition studies. Sufficient time points were provided on most runs such that turbulent, transitional, and laminar levels could be observed. Figure 6 presents data from two time points on a single run. Note that both laminar and turbulent levels are in good agreement with theory. One should also note the tendancy to "relaminarize" at $s/r_n = 1.6$. This phenomenon was observed on most runs and was particularly strong at the $s/r_n = 1.6$ location.

The variation of wall pressure and heat-transfer rate at the aft end of the model, with angle of attack, is shown in Fig. 7. The pressure data vary as expected with angle of attack, and the $\alpha = 0$ level is slightly above inviscid method of characteristic theory also, as expected. These data indicate a symmetrical flow field without measurable angularity. This confirms operational measurements made before each run which indicated that the model was at the expected attitude within ±0.1 deg. Heat-transfer measurements (Fig. 7b) vary linearly with angle of attack.

Transition is depicted at three separate model stations in Fig. 8 by examining the variation of heat-transfer ratio ($\dot{q}/\dot{q}_o$) with free-stream unit Reynolds number. Turbulent, transitional, and laminar regimes are easily identified for this case of $\alpha = 0$ and mass flow ($\dot{m}$) of zero. Note that a fully turbulent level is apparently established on the nose section at $\theta = 60$ deg and at $s/r_n = 1.6$ station, providing the Reynolds number is above 10 million per foot. At the $s/r_n = 6.01$ station, a fully turbulent level is established at a Reynolds number of 6 million per foot as shown in Fig. 8c. Generally speaking, the data obtained at the 6.01 station was typical of all stations on the aft conical section. The large amount of scatter noted in the transition regions is caused by asymmetric transition. This phenomena was caused in part by the relatively rough surface of the model brought about by (1) glue residues which could not be removed without breaking the seal on the model surface and/(2) the gage installation discontinuities resulting from the requirement of not touching the model surface with tools as would normally be done in fairing gages smooth.

Figure 9 presents similar results for the case of $\alpha = 2$ deg and $\dot{m} = 0$. By comparing Fig. 9 with the $\alpha = 0$ results from Fig. 8 (illustrated with shaded data bands), the effect of angle of attack on transition is observed. The expected windward-leeward bias in the heat-transfer results (caused by angle of attack) is to be noted. This trend is in agreement with the results presented in Ref. 10.

The quoted mass flow rates are total mass flow to the model chamber. Figure 10 indicates the effects of the highest mass addition ($\dot{m} = 0.042$ lbm/sec) on heat-transfer results at the $s/r_n = 1.6$ station. Apparent turbulent levels were established at a lower unit Reynolds number with this highest mass addition present. This particular station ($s/r_n = 1.6$) is typical of results on the nose section with 0.042 lbm/sec mass addition. Mass addition to the boundary layer through the nose section at lower rates did not change the location of transition significantly

from the no-blowing condition. Angle of attack did not influence the location of transition with 0.042 lbm/sec mass addition present. The maximum of 0.0044 lbm/sec on the aft cone section did not produce measureable changes.

6.0 SUMMARY OF RESULTS

Results of the test conducted on an $r_n/r_b = 0.5$, 9.75-deg half-angle, $r_b = 4.4$-in. sphere cone featuring porous skins are presented below. Heat-transfer-rate and pressure measurements were made at Mach number 7 with and without mass addition.

1. Variations of Reynolds number during a run permitted observation of laminar, transitional, and turbulent heat-transfer levels along the model surface.

2. Laminar and turbulent heat-transfer levels were in good agreement with theory for the $\dot{m} = 0$ and $\alpha = 0$ condition.

3. A unit Reynolds number of 10 million was required to produce an apparent turbulent heat-transfer level on the nose section.

4. As expected, transition locations were dependent on angle of attack for the range of angles tested (0 to 5 deg).

5. A mass flow rate of 0.042 lbm/sec through the forward model chamber was required to produce significant effects on the location of transition.

REFERENCES

1. Test Facilities Handbook (Tenth Edition). "von Kármán Gas Dynamics Facility, Vol. 3." Arnold Engineering Development Center, May 1974.

2. Pate, S. R. and Eaves, R. H., Jr. "Recent Advances in the Performance and Testing Capabilities of the AEDC-VKF Tunnel F (HOTSHOT) Hypersonic Facility." AIAA Paper No. 74-84, Presented at the AIAA 12th Aerospace Sciences Meeting, Washington, D. C., January 30 - February 1, 1974.

3. Ledford, R. L., Smotherman, W. E., and Kidd, C. T. "Recent Developments in Heat-Transfer-Rate, Pressure, and Force Measurements for Hotshot Tunnels." AEDC-TR-66-228 (AD645764), January 1967.

4. Bynum, D. S. "Instrumentation for the AEDC/VKF 100-in. Hotshot (Tunnel F)." AEDC-TR-66-209 (AD804567), January 1967.

5. Fay, J. A. and Riddell, F. R. "Theory of Stagnation Point Heat Transfer in Dissociated Air." Journal of the Aeronautical Sciences, Vol. 25, No. 2, February 1958, pp. 73-85, 121.

6. Brahinsky, Herbert S. and Neel, Charles A. "Tables of Equilibrium Thermodynamic Properties of Nitrogen." Vol. I-IV, AEDC-TR-69-126, August 1969.

7. Griffith, B. J. and Lewis, Clark H. "Laminar Heat-Transfer to Spherically Blunted Cones at Hypersonic Conditions." AIAA Journal, Vol. 2, No. 3, March 1964, pp. 438-444.

8. Grabau, Martin, Smithson, H. K., Jr., and Little, W. J. "A Data Reduction Program for Hotshot Tunnels Based on the Fay-Riddell Heat-Transfer Rate Using Nitrogen at Stagnation Temperatures from 1500 to 5000°K." AEDC-TDR-64-50 (AD601070), June 1964.

9. Mayne, A. W., Jr. and Dyer, D. F. "Comparison of Theory and Experiment for Turbulent Boundary Layers on Simple Shapes at Hypersonic Conditions." Proceedings of the 1970 Heat-Transfer and Fluid Mechanics Institute, Stanford University Press, 1970, pp. 168-188.

10. Potter, J. Leith. "The Unit Reynolds Number Effect on Boundary Layer Transition." Ph. D. Dissertation, Vanderbilt University, Nashville, Tenn., May 1974.

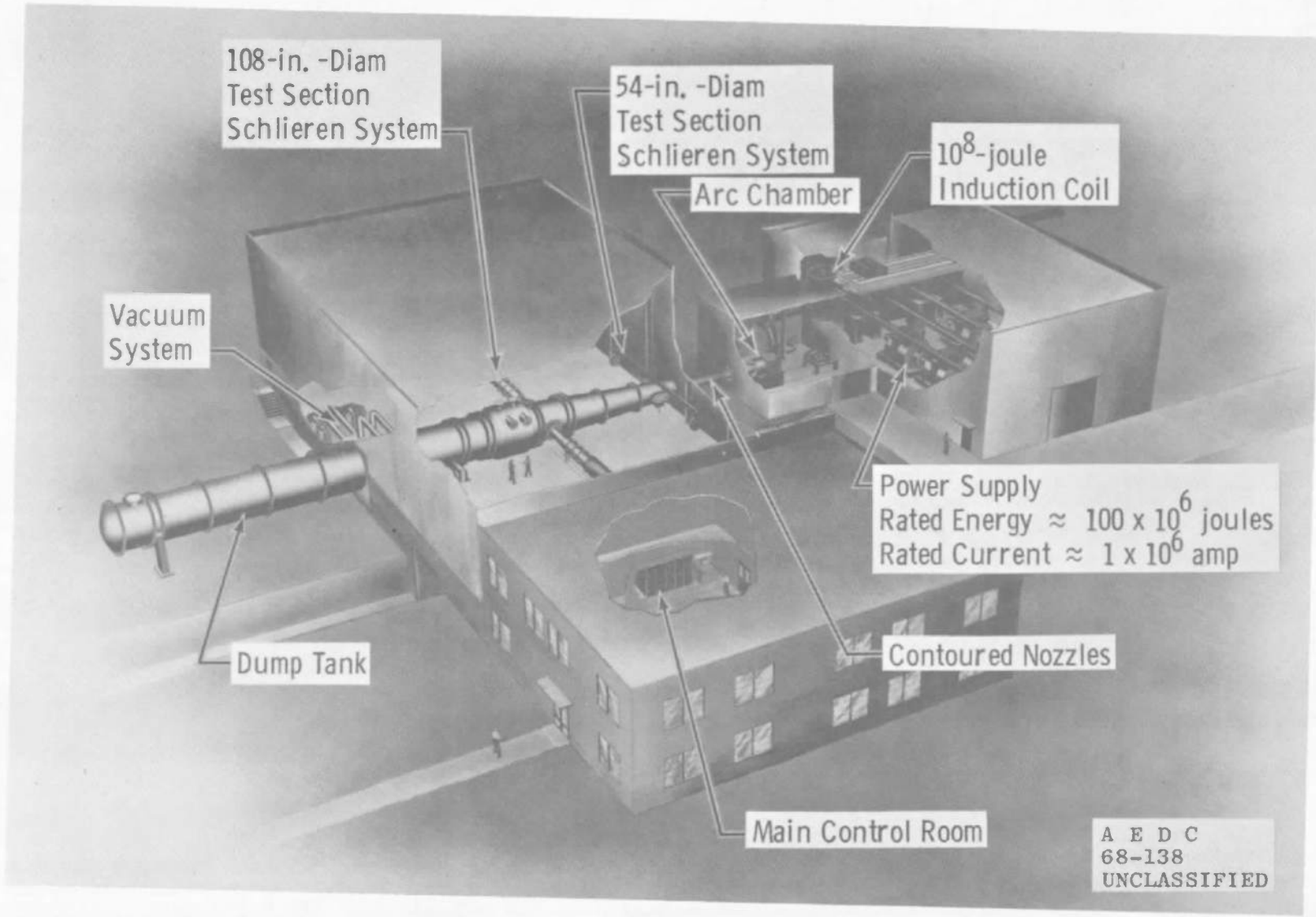

Figure 1. AEDC-VKF Tunnel F plant.

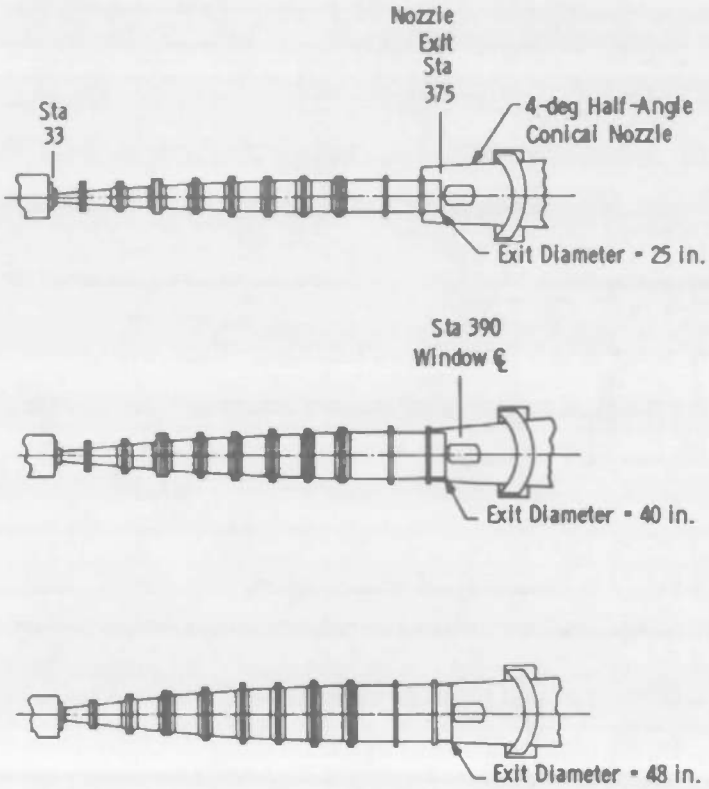

Figure 2. Tunnel F family of contoured nozzles.

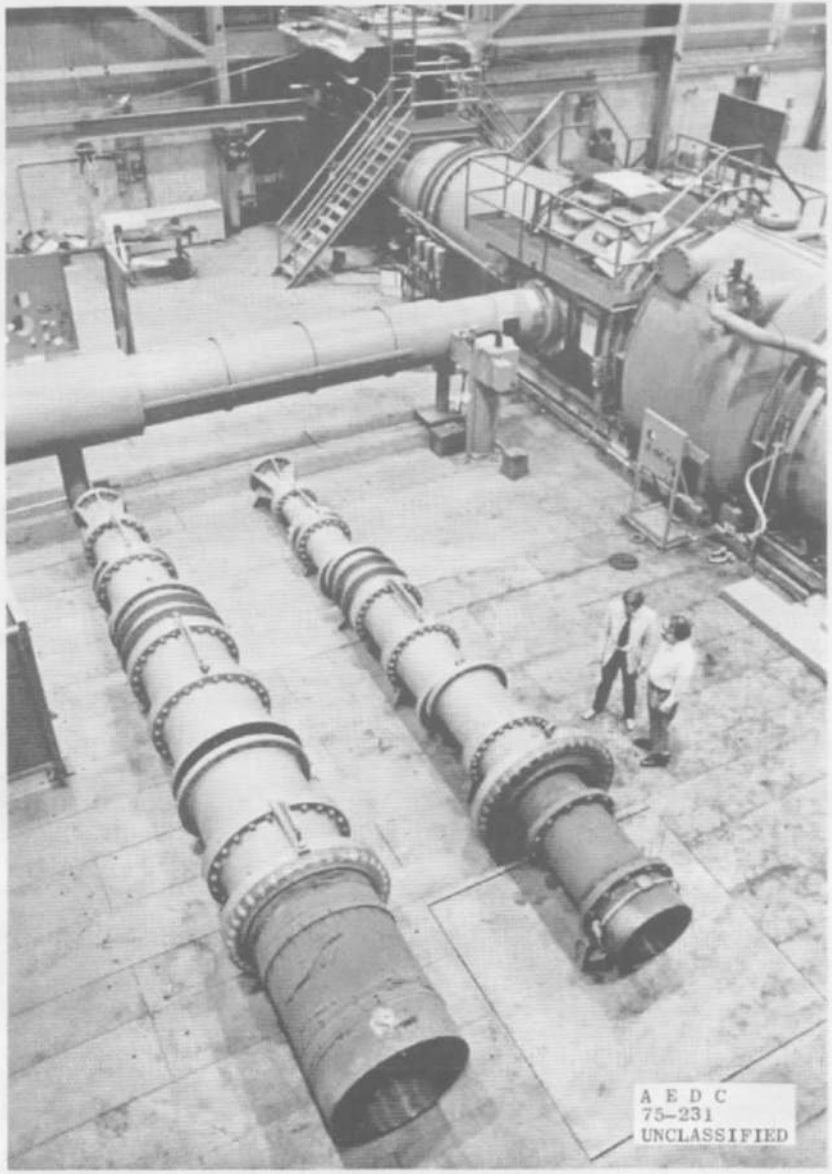

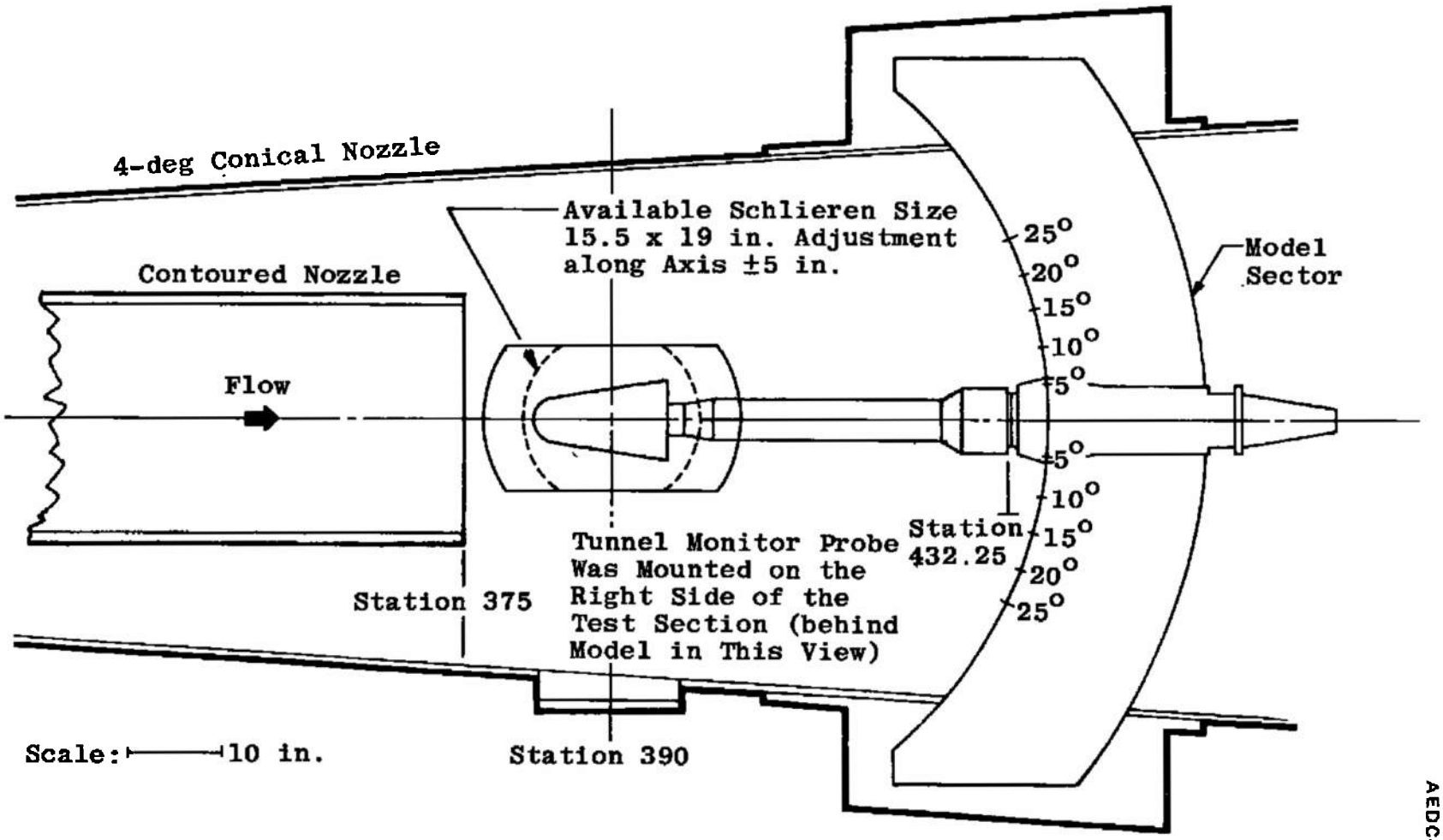

Figure 3. Model installation.

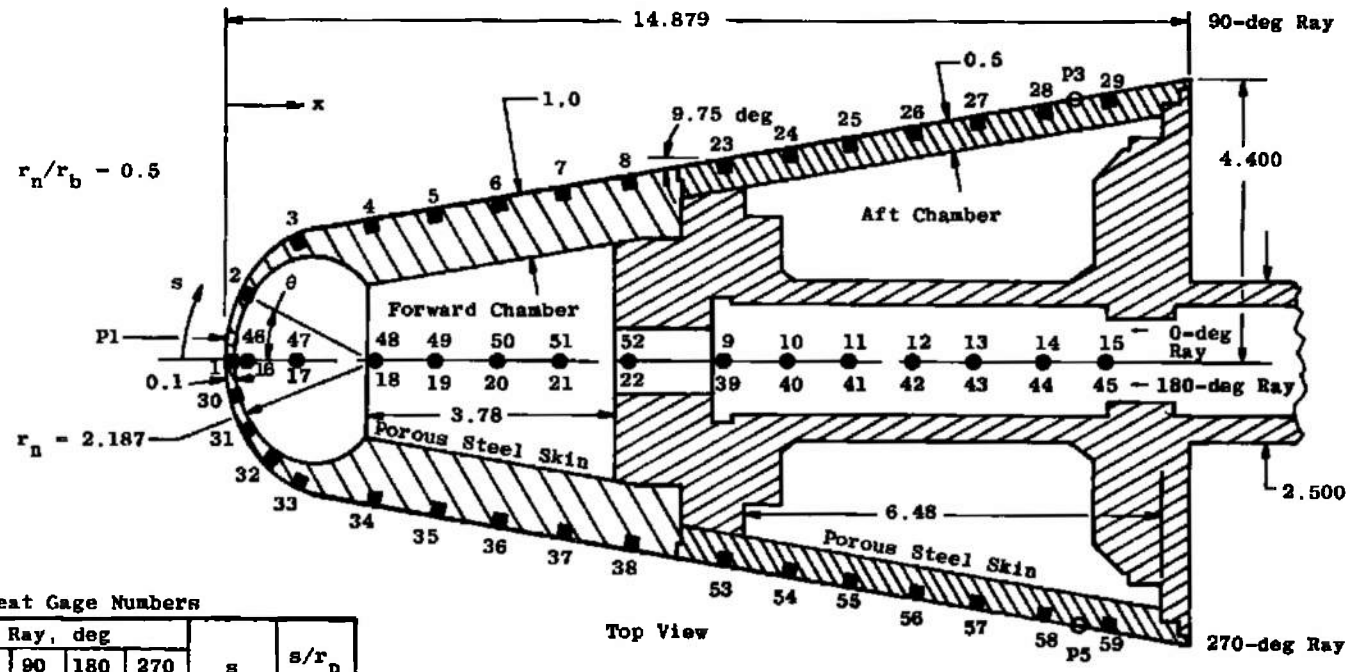

Heat Gage Numbers

	Station	Ray, deg 0	90	180	270	s	s/r_n
θ	0	-	1	-	-	0	0
	15	-	-	-	30	0.57	0.26
	30	46	2	16	31	1.15	0.52
	45	-	-	-	32	1.72	0.79
	60	47	3	17	33	2.29	1.05
x	2.25	48	4	18	34	3.50	1.60
	3.25	49	5	19	35	4.52	2.07
	4.25	50	6	20	36	5.53	2.53
	5.25	51	7	21	37	6.55	2.99
	6.25	52	8	22	38	7.56	3.46
	7.75	9	23	39	53	9.08	4.15
	8.75	10	24	40	54	10.01	4.62
	9.75	11	25	41	55	11.11	5.08
	10.75	12	26	42	56	12.13	5.55
	11.75	13	27	43	57	13.14	6.01
	12.75	14	28	44	58	14.16	6.47
	13.75	15	29	45	59	15.17	6.94

Pressure Gage Numbers

Station	Ray, deg 0	90	180	270	s	s/r_n
θ = 10 deg	-	1	-	-	0.38	0.17
x = 13.25	2	3	4	5	14.66	6.70

Figure 4. Model details.

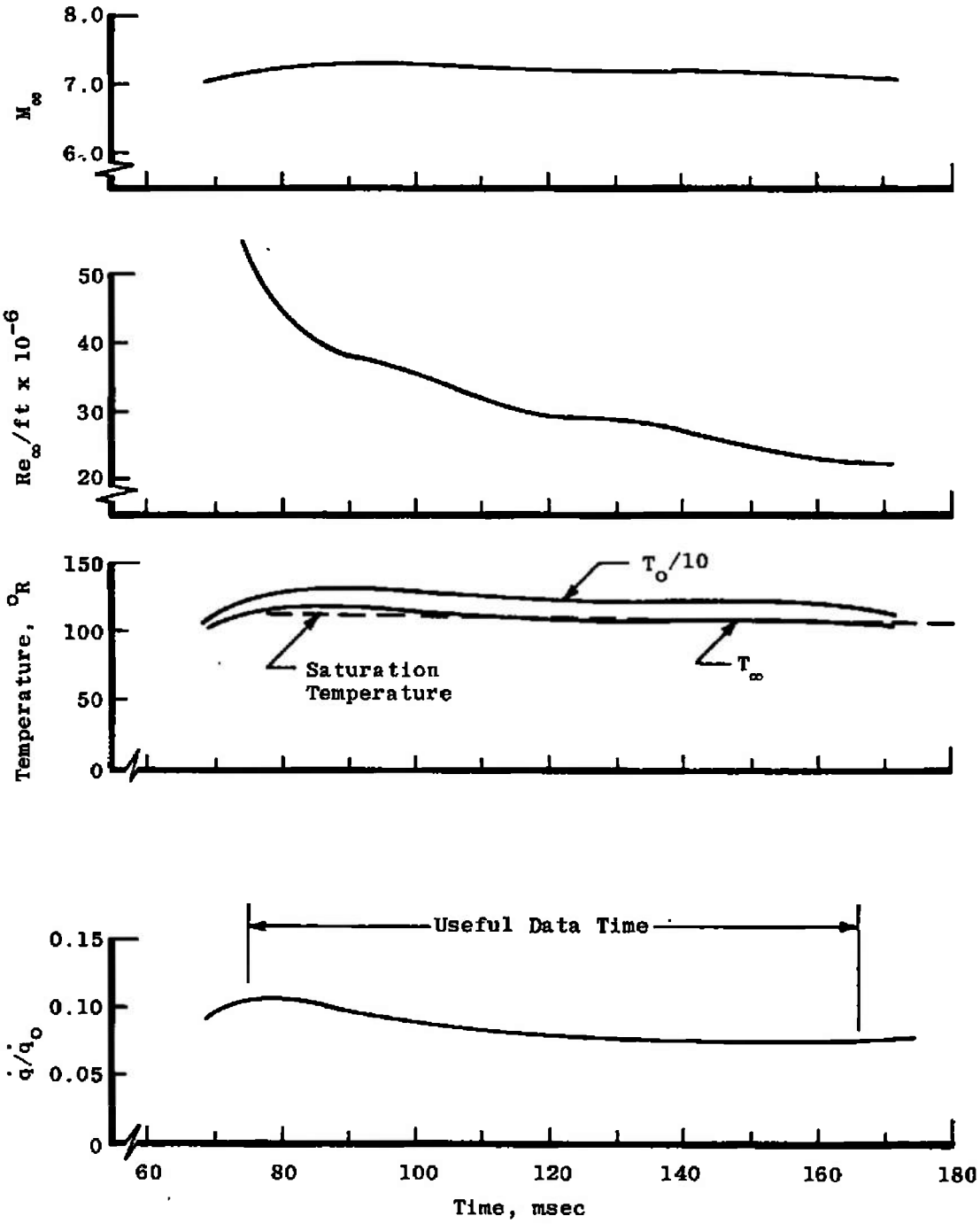

Figure 5. Typical timewise test conditions and data.

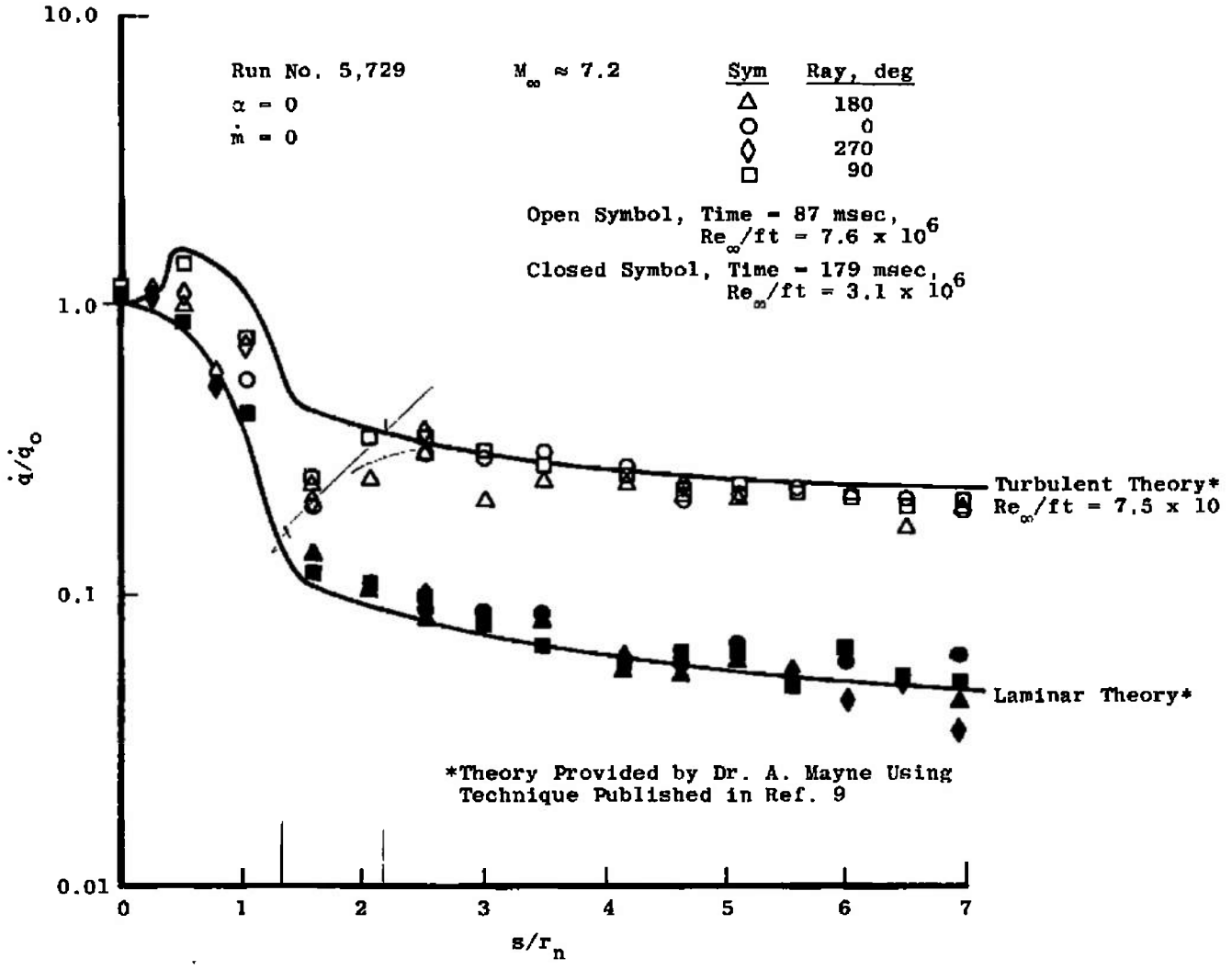

Figure 6. Comparison of experimental data and theory.

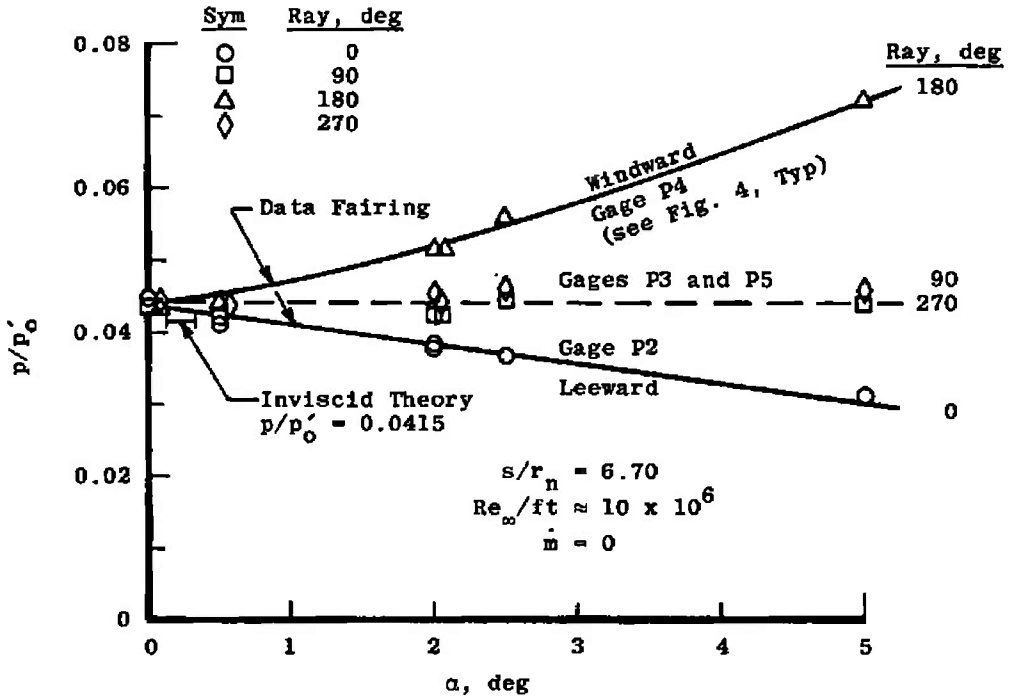

a. Pressure versus α

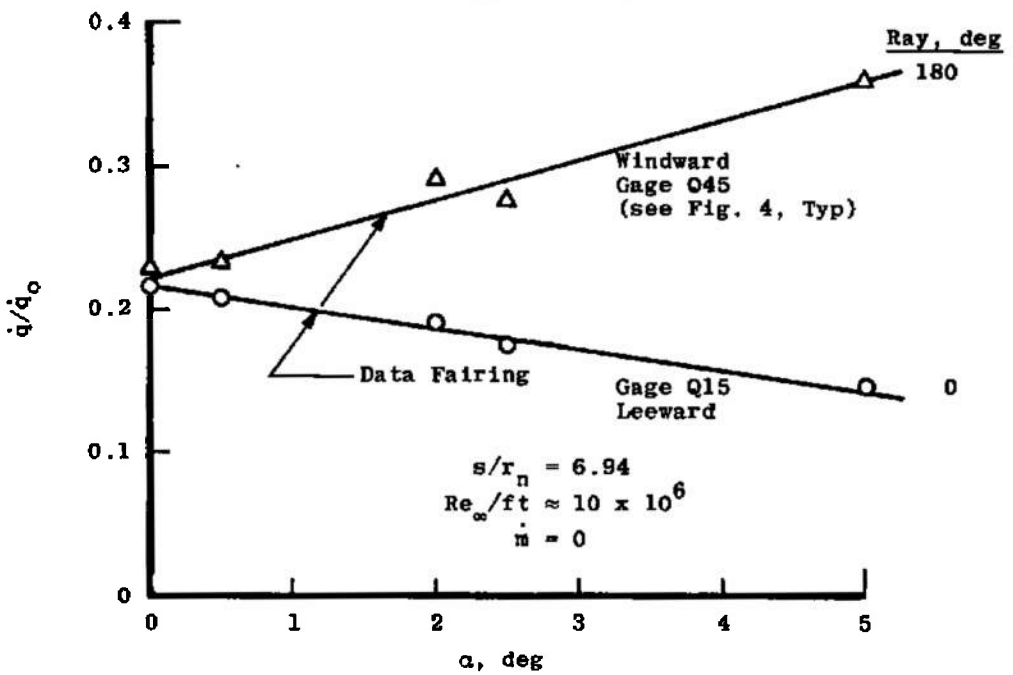

b. Turbulent $\dot{q}$ versus α

Figure 7. Angle-of-attack effect on pressure and heat transfer.

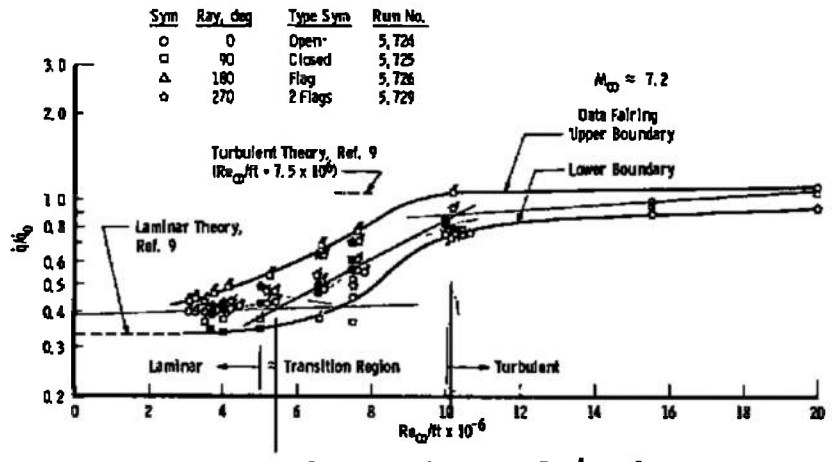

a. θ = 60-deg station, α = 0, $\dot{m}$ = 0

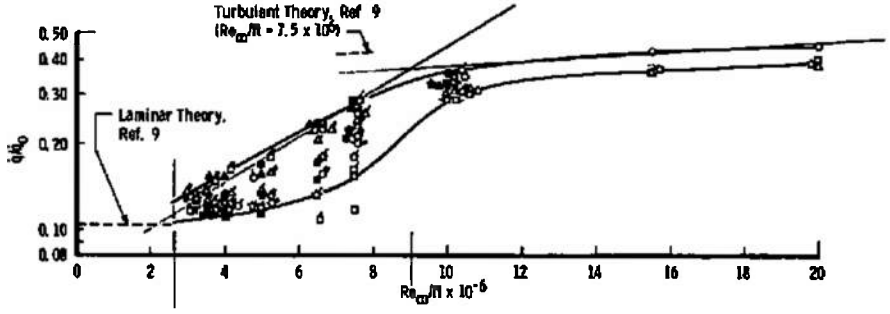

b. s/r_n = 1.6 station, α = 0, $\dot{m}$ = 0

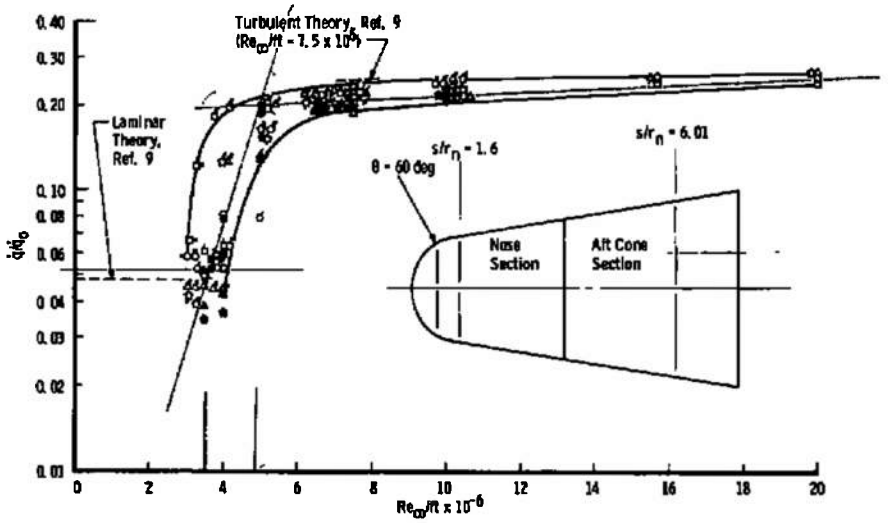

c. s/r_n = 6.01 station, α = 0, $\dot{m}$ = 0

Figure 8. Boundary-layer transition results for α = 0, $\dot{m}$ = 0.

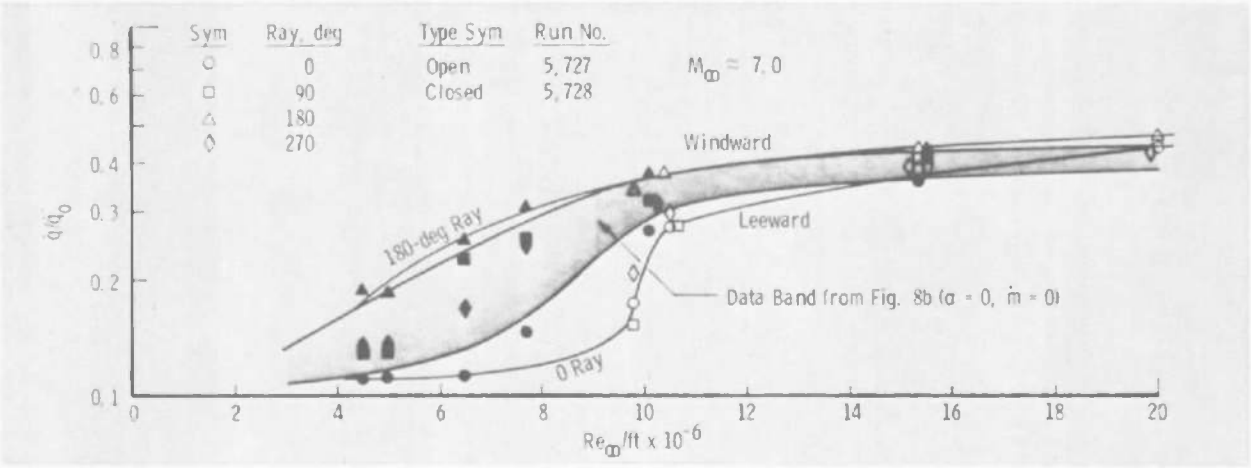

a. s/r_n = 1.6 station, α = 2 deg, $\dot{m}$ = 0

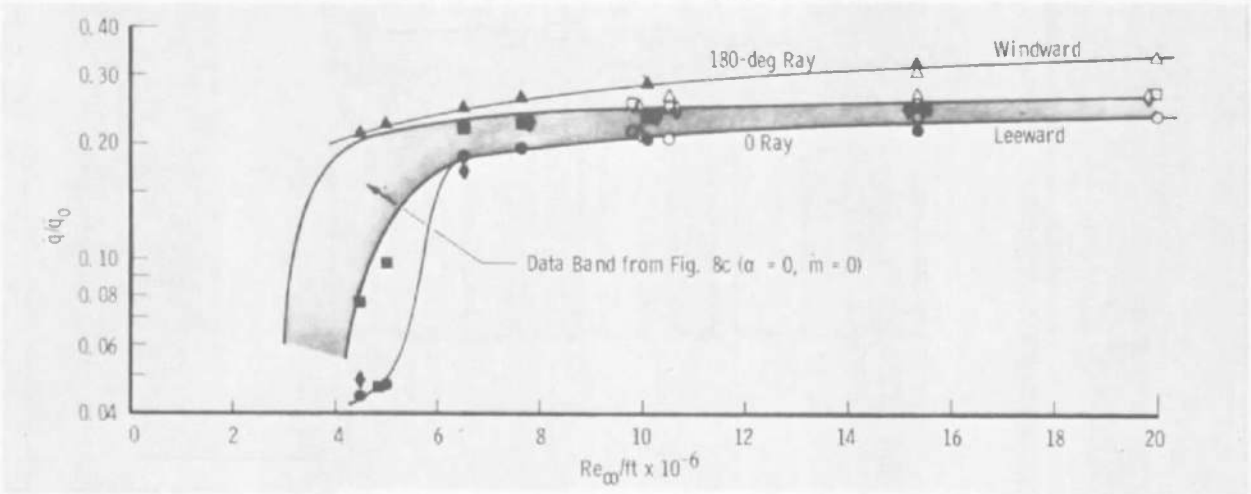

b. s/r_n = 6.01 station, α = 2 deg, $\dot{m}$ = 0

Figure 9. Boundary-layer transition results for α = 2 deg, $\dot{m}$ = 0.

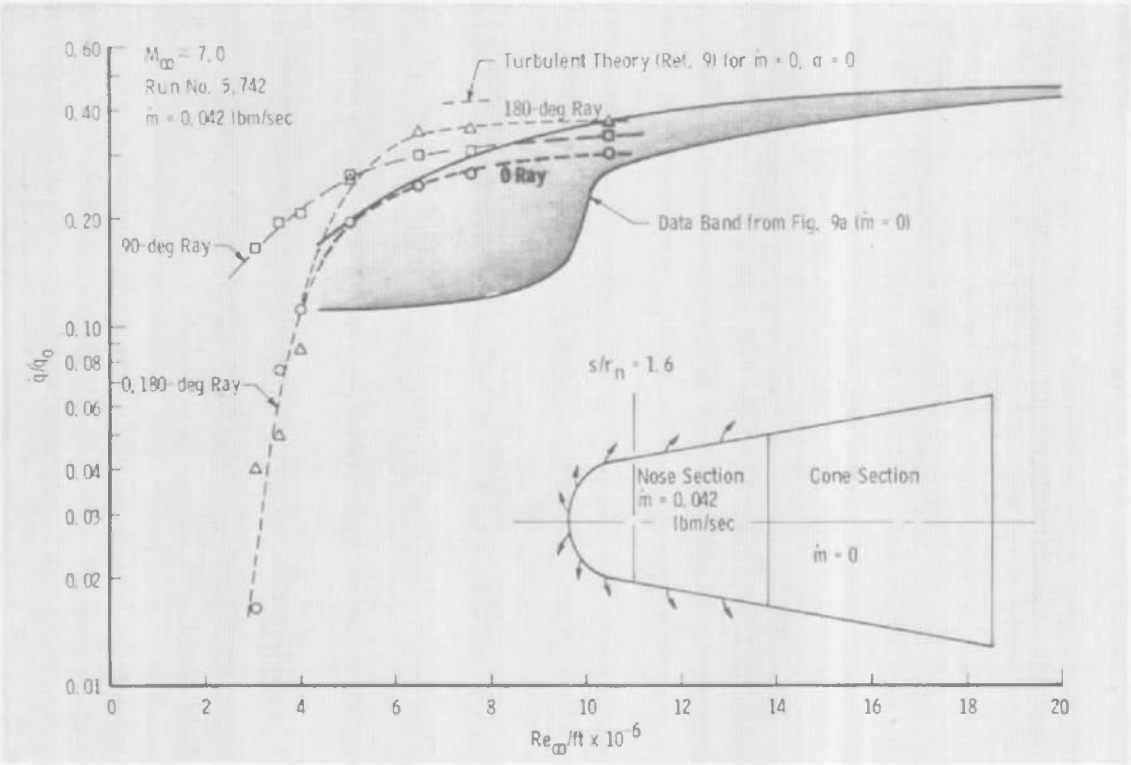

a. α = 2 deg, $\dot{m}_{nose}$ = 0.042 lbm/sec

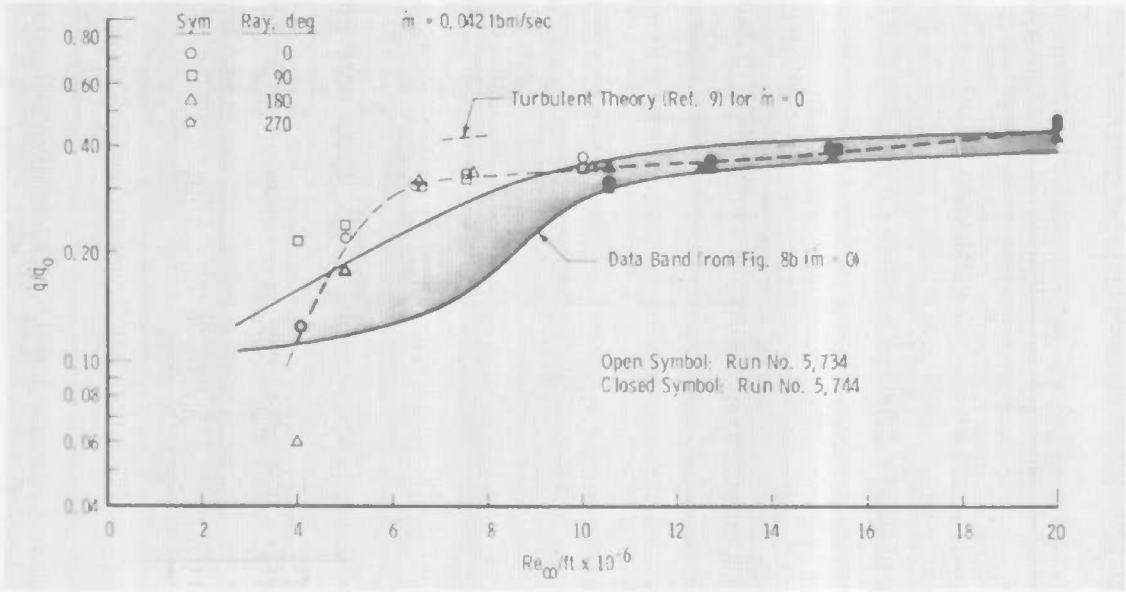

b. α = 0, $\dot{m}_{nose}$ = 0.042 lbm/sec

Figure 10. Effects of mass addition on boundary-layer transition at s/r_n = 1.6.

Table 1. Test Summary

Run No.	α, deg	Re_∞/ft Min	Re_∞/ft Max	$\dot{m}$, nose, lbm/sec	$\dot{m}$, cone, lbm/sec
5,729	0	2.8	10.2	0	0
5,725	↓	3.6	10.0	↓	↓
5,726		3.0	15.6		
5,724		6.5	19.8		
5,745	↓	15.1	40.5		
5,730	0.5	3.5	10.3		
5,731	0.5	4.1	9.9		
5,727	2.0	9.0	20.4		
5,728	2.0	4.2	15.2		
5,737	2.5	3.5	10.2		
5,738	5.0	3.5	10.1	↓	↓
5,739	0	2.3	10.8	0.00432	0.00440
5,732	↓	2.9	9.6	0.00375	0
5,733		3.1	9.9	0.00400	0.00240
5,734		3.8	15.6	0.04211	0
5,735		2.5	10.1	0.00103	0.00088
5,736		3.5	15.6	0.00823	↓
5,744	↓	10.1	20.3	0.04187	
5,743	0.5	2.4	10.4	0.00835	
5,740	2.0	2.5	10.1	0.00415	
5,741	↓	2.5	10.2	0.00853	
5,742		2.7	10.4	0.04235	↓

NOMENCLATURE

h_o	Total enthalpy of gas, Btu/lbm
M_∞	Free-stream Mach number
$\dot{m}$	Mass flow rate, lbm/sec
p	Model pressure, psia
p_∞	Freestream static pressure, psia
p_o'	Total pressure behind the normal shock, psia
$\dot{q}$	Heat-transfer rate, Btu/ft^2-sec
$\dot{q}_o$	Stagnation heat-transfer rate on a hemisphere cylinder, $\dot{q}_o$ referenced to 2.187-in. radius
R	Gas constant
r_b	Model base radius, in.
Re_∞/ft	Free-stream unit Reynolds number, per ft
r_n	Model nose radius, in.
s	Surface distance, in.
s_∞	Free-stream entropy
T_∞	Free-stream static temperature, °R

T_o Reservoir temperature, °R

T_w Model wall temperature, °R

x Axial length measured from stagnation point, in.

α Model angle of attack, deg

θ Angle measured from the stagnation point to any gage on the model nose, deg